JOURNAL OF SOLID STATE CHEMISTRY 117, 206–212 (1995)

Cation Substitution in the Alluaudite Structure Type: Synthesis and Structure of $AgMn_3(PO_4)(HPO_4)_2$

F. Leroux, A. Mar, D. Guyomard, and Y. Piffard[1]

Institut des Matériaux, Laboratoire de Chimie des Solides, UMR 110 CNRS-Université de Nantes, 2 rue de la Houssinière, 44072 Nantes Cedex 03, France

Received July 21, 1994; in revised form December 13, 1994; accepted December 19, 1994

Silver manganese(II) phosphate bis(hydrogenphosphate), $AgMn_3(PO_4)(HPO_4)_2$, a synthetic unoxidized variant of the alluaudite group, has been prepared hydrothermally and its structure has been determined from single-crystal diffraction data. It crystallizes in space group $C2/c$ of the monoclinic system with $Z = 4$ in a cell of dimensions $a = 12.263(1)$, $b = 12.446(1)$, $c = 6.649(1)$ Å, and $\beta = 114.708(8)°$. The structure is similar to that of $NaMn_3(PO_4)(HPO_4)_2$, consisting of a complex network of edge-sharing $Mn(II)O_6$ octahedral chains that are linked together by both corner-sharing PO_4 tetrahedra and O–H ··· O bonds, forming tunnels along which Ag atoms reside. The principal difference arises in the occurrence of two sites for the Ag atoms, each partially occupied. The existence of a protonated series of alluaudites is implicated, to be contrasted with the natural alluaudites which are nonprotonated. A discussion on the differences between these two series is presented. © 1995 Academic Press, Inc.

INTRODUCTION

The alluaudite structure type encompasses a large group of transition-metal phosphate minerals. Through many years of analysis on natural alluaudites, Moore (1, 2) established an admirable systematization of their crystal chemistry. Writing in order of decreasing cation size, he proposed the general formulation $X(2)X(1)M(1)M(2)_2(PO_4)_3$ (with $Z = 4$), the most common constituents being $X(2) = Na^+, \square$; $X(1) = Na^+, Ca^{2+}$; $M(1) = Mn^{2+}, Fe^{2+}$; and $M(2) = Fe^{3+}, Fe^{2+}, Mn^{2+}$. Because the cations are invariably disordered among the different possible sites in natural alluaudites, there is an impetus to study synthetic alluaudites whose compositions represent end-members of series, in order to attain a fuller understanding of site preferences. Besides the original Buranga alluaudite, roughly of the composition $NaMnFe_2(PO_4)_3$ (1), the only other alluaudites that have been fully characterized by single-crystal X ray diffraction are $NaCdIn_2(PO_4)_3$ (3), $NaFe_3(PO_4)_3$ (4), $Na_2Fe_3(PO_4)_3$ (5), and $Cu_{1.35}Fe_3(PO_4)_3$ (6). Recently we demonstrated with the preparation of $NaMn_3(PO_4)(HPO_4)_2$ (7), the first example of an all-manganese form of alluaudite, that H^+ cations may also be incorporated into the structure, and we also pointed out that this was an example of a completely unoxidized variant of alluaudite. We report here the preparation and structure of the first silver substituted analogue, $AgMn_3(PO_4)(HPO_4)_2$, and describe its relationship to the other known alluaudites. This examination prompted a reevaluation of the previously reported compound $NaFe_3(PO_4)_3$ (4), suggesting that it too is in fact a protonated form of alluaudite. With these examples, we begin to see the emergence of a protonated series of alluaudites that is distinct from the nonprotonated series.

EXPERIMENTAL

Synthesis. Crystals of $AgMn_3(PO_4)(HPO_4)_2$ were prepared by the hydrothermal synthesis, under conditions similar to those in the preparation of $NaMn_3(PO_4)(HPO_4)_2$ (7). A mixture of $H_2Mn_4O_9 \cdot xH_2O$ (rancieite (8)) (410 mg, 1.0 mmol), H_3PO_4 (10 mmol, 1.0 *M*), $AgNO_3$ (679 mg, 4.0 mmol), and 1,4-diazabicyclo[2.2.2]-octane (DABCO) (224 mg, 2.0 mmol) was placed in a Teflon vessel which was filled 80% with water (final pH 1–2) and enclosed in a stainless steel bomb. The mixture was heated at 180°C under autogenous pressure for 1 week. The major product of the reaction was $AgMn_3(PO_4)(HPO_4)_2$, which crystallizes as thin colorless needles; these crystals were confirmed by microprobe analysis on a scanning electron microscope to contain Ag, Mn, and P in an atomic ratio of 1 : 3 : 3. The product is contaminated with excess elemental silver, present as a fine gray powder, and $Mn_7(HPO_4)_4(PO_4)_2$ (9), recognizable as thick blocks (< ~2%—not visible in the XRD diagram).

Attempts to prepare a Tl or K analogue were unsuccessful, these reactions tending to yield $Mn_5(HPO_4)_2(PO_4)_2 \cdot 4H_2O$ (10–12) instead. The inability to incorporate these cations into the alluaudite structure may imply a limiting size that can be accommodated in the $X(2)'$ site (*vide infra*).

[1] To whom correspondence should be addressed.

0022-4596/95 $6.00

Structure determination. Initial photographic work immediately revealed the similarity of $AgMn_3(PO_4)(HPO_4)_2$ with $NaMn_3(PO_4)(HPO_4)_2$. The cell parameters were refined from powder diffraction data collected on an INEL multidetector system ($\lambda(CuK\alpha_1) = 1.54056$ Å; Si standard). Table 1 lists observed and calculated interplanar distances, and the intensities calculated from the crystal structure with the use of the program LAZY-PULVERIX (13). Single-crystal intensity data were collected at room temperature on a Siemens P4 diffractometer under the conditions given in Table 2. Data reduction and refinements were carried out with the use of programs in the SHELXTL PLUS package (14). The systematic absences (hkl, $h + k = 2n + 1$; $h0l$, $l = 2n + 1$) are consistent with the space groups $C2/c$ and Cc, and the space group $C2/c$ was chosen based on analogy with $NaMn_3(PO_4)(HPO_4)_2$. Conventional atomic scattering factors and anomalous dispersion corrections were used. An empirical absorption correction based on psi scans was applied to the data (min/max trans. = 0.81/0.88). Initially, the position of the Ag, Mn, P, and O atoms were taken from the corresponding positions in $NaMn_3(PO_4)(HPO_4)_2$ (7). The structure was then refined by least-squares methods. Inspection of the difference Fourier map suggested that the Ag site must in fact be split into two closely separated sites about 0.4 Å apart. Based on a model imposing no particular constraints on the occupancies and thermal factors of two independent Ag sites, the refinement converged to yield, for Ag(1) and Ag(2), occupancies of 52(4) and 46(4)%, respectively, and isotropic thermal factors (U) of 0.014(2) and 0.017(2) Å^2, respectively. As the sum of the Ag occupancies is essentially 100%, in agreement with the expected formula $AgMn_3(PO_4)(HPO_4)_2$ and the microprobe analysis, and as there is no reason to suspect nonstoichiometry, in subsequent refinements the sum of Ag occupancies was fixed to be exactly 100% and the thermal factors of Ag(1) and Ag(2) were constrained to be identical. A refinement performed in this manner converges to the same result as earlier, offering no improvement in the residual ($R = 0.042$) compared to that of the previous refinement ($R = 0.041$) but with significantly smaller standard deviations for the occupancies and thermal factors. As was the case in $NaMn_3(PO_4)(HPO_4)_2$ (7), the existence of an O–H ··· O bridge between O(2) and O(4) is suggested by their anomalously low bond valence sums (15, 16) of 1.50 and 1.31, respectively, compared to the expected value of 2 (Table 3). The difference electron density map reveals some poorly resolved subsidiary electron density between O(2) and O(4), but the data were deemed inadequate to warrant treatment of an H atom in the refinement. The final cycle of refinement on F on 548 reflections with $I > 2\sigma(I)$ and 42 variables (including an extinction parameter), with isotropic thermal parameters for all atoms, resulted in

TABLE 1
X Ray Powder Diffraction Data for $AgMn_3(PO_4)(HPO_4)_2$

h	k	l	d_{obs} (Å)	d_{calc} (Å)	I/I_o	h	k	l	d_{obs} (Å)	d_{calc} (Å)	I/I_o
1	1	0	8.305	8.301	100	1	5	$\bar{1}$	2.184	2.186	3
2	2	0	4.153	4.150	3	4	4	$\bar{1}$		2.182	4
2	2	$\bar{1}$	4.061	4.062	3	3	1	3	2.162	2.162	8
1	3	0	3.887	3.888	28	2	2	2	2.144	2.145	3
2	0	$\bar{2}$	3.294	3.294	11	0	6	0	2.075	2.074	3
1	1	$\bar{2}$	3.174	3.173	8	3	5	0	2.068	2.068	3
1	3	1	3.073	3.072	21	5	3	$\bar{2}$	2.021	2.020	12
0	0	2	3.020	3.020	20	0	6	1	1.962	1.962	4
3	1	$\bar{2}$	2.960	2.961	25	3	3	$\bar{3}$	1.942	1.941	5
3	3	$\bar{1}$	2.879	2.878	6	2	6	$\bar{1}$	1.933	1.935	4
4	0	0	2.785	2.785	19	6	0	0	1.857	1.857	5
3	3	0	2.767	2.767	46	2	4	$\bar{3}$	1.803	1.803	3
0	4	1		2.766	11	3	3	2	1.782	1.782	11
2	4	0	2.716	2.716	41	2	6	1	1.776	1.776	3
4	0	$\bar{2}$	2.680	2.680	25	1	7	0	1.755	1.756	3
1	1	2	2.591	2.591	19	1	7	$\bar{1}$	1.717	1.717	4
1	3	$\bar{2}$	2.574	2.574	29	1	3	3	1.691	1.690	3
2	0	2	2.285	2.285	7	6	4	$\bar{2}$	1.681	1.681	10
5	1	$\bar{2}$	2.275	2.274	5	2	0	4	1.641	1.641	11
1	3	2	2.233	2.232	3	4	6	$\bar{2}$		1.640	4
5	1	0	2.193	2.193	17	7	3	2	1.604	1.604	3
						6	4	0	1.594	1.594	3

TABLE 2
Crystal Data and Intensity Collection for $AgMn_3(PO_4)(HPO_4)_2$

Formula	$AgMn_3(PO_4)(HPO_4)_2$
Formula mass (amu)	559.61
Space group	$C2/c$
a (Å)	12.263(1)
b (Å)	12.446(2)
c (Å)	6.649(1)
β (°)	114.708(8)
V (Å^3)	921.9(2)
Z	4
ρ_c (g cm^{-3})	4.03
μ(Mo$K\alpha$) (cm^{-1})	67.0
Crystal dimensions	Needle, 0.01 × 0.01 × 0.22 mm
Radiation	Mo$K\alpha$, $\lambda = 0.7107$ Å
Scan mode	ω
Scan range (°)	$1.0 + \Delta\theta(\alpha_1, \alpha_2)$
2θ limits (°)	2.0–60.0
Data collected	$-1 \le h \le 17$, $-1 \le k \le 17$, $-9 \le l \le 8$
Number of data collected	1668
Number of unique data	1307 ($R_{int} = 0.021$)
Number of unique data, with $I > 2\sigma(I)$	548
Number of variables	42
$R(F)^a$	0.042
$R_w(F)^b$	0.026
GOF	0.96

[a] $R(F) = \Sigma \|\|F_o| - |F_c\|| / \Sigma |F_o|$.
[b] $R_w(F) = [\Sigma w(|F_o| - |F_c|)^2 / \Sigma w F_o^2]^{1/2}$ with $w = 1/\sigma^2(F)$.

TABLE 3
Bond Valence Sums for Atoms in $AgMn_3(PO_4)(HPO_4)_2$

Atom	V	Atom	V
Mn(1)	1.83	O(1)	1.82
Mn(2)	2.11	O(2)	1.50[a]
P(1)	4.72	O(3)	1.91
P(2)	4.69	O(4)	1.31[a]
Ag(1)	0.84	O(5)	1.93
Ag(2)	0.94	O(6)	1.93, 1.98[b]

[a] Bonded to H atom (not located).
[b] With Ag(1) and Ag(2) environment, respectively.

residuals of $R = 0.042$ and $R_w = 0.026$. The final difference electron density map shows extrema of $(\Delta\rho)_{max} = 1.2$ and $(\Delta\rho)_{min} = -1.2\ e^-\ Å^{-3}$. Final values of the positional and thermal parameters are given in Table 4. A list of structure amplitudes is available as supplementary material. Table 5 lists relevant interatomic distances and angles in $AgMn_3(PO_4)(HPO_4)_2$.

Physical measurements. Infrared spectra were obtained on a 20SCX FTIR spectrometer with the use of KBr pellets. Thermal measurements were made on a Perkin–Elmer TGS-2 thermogravimetric analyzer.

RESULTS AND DISCUSSION

Before proceeding, it is useful to recall the general crystal chemical formulation for the alluaudite structure type, $X(2)X(1)M(1)M(2)_2(PO_4)_3$. Thus, although the formula $AgMn_3(PO_4)(HPO_4)_2$ is brief and places emphasis on the existence of $(HPO_4)^{2-}$ groups, we will have recourse to writing it as explicitly as $Ag^+(H^+)_2Mn^{2+}(Mn^{2+})_2(PO_4)_3$ to draw attention to the identity of the cations and their oxidation states, as shown in Table 6.

TABLE 4
Positional and Isotropic Thermal Parameters for $AgMn_3(PO_4)(HPO_4)_2$

Atom	Wyckoff position	x	y	z	U_{iso} (Å^2)[a]
Ag(1)[b]	4e	0	0.041(1)	0.75	0.0173(5)
Ag(2)[b]	4e	0	0.011(1)	0.75	0.0173(5)
Mn(1)	4e	0	0.2828(2)	0.25	0.0109(7)
Mn(2)	8f	0.2907(2)	0.6607(2)	0.3752(3)	0.0081(5)
P(1)	4e	0	0.6798(4)	0.25	0.008(1)
P(2)	8f	0.2179(3)	0.8875(3)	0.1123(5)	0.0064(7)
O(1)	8f	0.4642(6)	0.7492(5)	0.544(1)	0.006(2)
O(2)	8f	0.1059(6)	0.6058(6)	0.266(1)	0.010(2)
O(3)	8f	0.3459(6)	0.6717(6)	0.108(1)	0.005(1)
O(4)	8f	0.1456(6)	0.4107(6)	0.344(1)	0.010(2)
O(5)	8f	0.2138(6)	0.8207(6)	0.300(1)	0.005(1)
O(6)	8f	0.3429(6)	0.4965(6)	0.397(1)	0.010(1)

[a] $U_{iso} = \langle u^2 \rangle$.
[b] Occ(Ag(1)) = 58(3)%; occ(Ag(2)) = 42(3)%.

Except for the placement of the $X(2)$ cations, the structure of $AgMn_3(PO_4)(HPO_4)_2$ is similar to that of $NaMn_3(PO_4)(HPO_4)_2$ (7), a protonated, unoxidized variant of alluaudite. While there are important differences between these and the nonprotonated alluaudites, the covalent framework (comprising MO_6 octahedra and PO_4 tetrahedra) is essentially the same in both cases. A detailed description of this complex arrangement has been given previously (1). Briefly, edge-sharing chains of $M(1)O_6$ and $M(2)O_6$ distorted octahedra running along the $[10\bar{1}]$ direction are linked by PO_4 tetrahedra to form "pleated sheets" lying parallel to the (010) plane (these can be seen edgewise in Fig. 1 aligned along $y = \pm\frac{1}{4}$), which in turn are linked together by corner-sharing an oxygen atom (O(6)) of a $P(2)O_4$ tetrahedron in one sheet with a $M(2)O_6$ octahedron of an adjacent sheet.

The salient feature of the structure that is important for our discussion is the occurrence of tunnels that are outlined by the covalent framework and occupied by the alkali or pseudo-alkali cations $X(1)$ and $X(2)$. Two types of tunnels run through the structure, as indicated in Fig. 1: tunnel 1 along $(\frac{1}{2}, 0, z)$ and $(0, \frac{1}{2}, z)$, and tunnel 2 along $(0, 0, z)$ and $(\frac{1}{2}, \frac{1}{2}, z)$. The location of the cation sites for $X(1)$ and $X(2)$ differs, however, between different alluaudites, as shown in Table 6.

Figure 2 shows the arrangement of oxygen atoms within tunnel 1. A cation situated at $A(1) = \frac{1}{2}, 0, 0$ resides in the center of a roughly cubic environment (Fig. 2a), as is the case for the Na atoms in $NaMnFe_2(PO_4)_3$ (1) and $NaCdIn_2(PO_4)_3$ (3), with Na–O distances ranging from 2.3 to 3.1 Å. In the protonated alluaudites, the H^+ cations are also located in this tunnel, in the form of hydrogen bonds forming bridges across O(2) and O(4) (Fig. 2b). The formation of the O(2)–H–O(4) bridge brings about a significant tightening of the cubic arrangement of oxygen atoms: Table 7 shows that the O(2)–O(4) distance has decreased from ~3.0 Å in the nonprotonated forms to ~2.5 Å in the protonated forms. Further evidence for O–H bonds in $AgMn_3(PO_4)(HPO_4)_2$ was found from the infrared spectrum which clearly shows the presence of broad O–H stretching and bending vibrations centered at 2200 and 1380 cm^{-1}.

Turning now to tunnel 2, we find that the same overall environment of oxygen atoms leads to two potential kinds of cation sites, as shown in Fig. 3: $A(2) = 0, 0, 0$, and $A(2)' = 0, \varepsilon, \frac{3}{4}$ (where ε is a small positive number). $A(2)$ is a highly irregular rhombic site, while $A(2)'$ is an off-centered square planar site. With two short $A(2)$–O(6) distances (Table 7), $A(2)$ must really be considered to be linear, the next two short $A(2)$–O(1) distances being much larger. Formerly it has always been assumed that it

TABLE 5
Selected Interatomic Distances (Å) and Angles (°) in $AgMn_3(PO_4)(HPO_4)_2$

Mn atom environments

Mn(1)	O(1)[i]	O(1)[ii]	O(3)[i]	O(3)[ii]	O(4)	O(4)[iii]
O(1)[i]	2.214(8)	4.35(2)	2.816(9)	3.05(1)	3.64(1)	3.099(9)
O(1)[ii]	*158.2(4)*	2.214(8)	3.05(1)	2.816(9)	3.099(9)	3.64(1)
O(3)[i]	*79.1(3)*	*87.3(3)*	2.209(7)	3.45(1)	4.47(1)	2.99(1)
O(3)[ii]	*87.3(3)*	*79.1(3)*	*102.5(4)*	2.209(7)	2.99(1)	4.47(1)
O(4)	*108.2(3)*	*87.3(3)*	*170.9(2)*	*83.6(3)*	2.276(7)	3.25(1)
O(4)[iii]	*87.3(3)*	*108.2(3)*	*83.6(3)*	*170.9(2)*	*91.2(4)*	2.276(7)

Mn(2)	O(1)	O(2)	O(3)	O(5)	O(5)[iv]	O(6)
O(1)	2.237(7)	4.37(1)	2.816(9)	2.948(9)	2.92(1)	3.44(1)
O(2)	*163.7(3)*	2.180(7)	3.61(1)	2.95(1)	2.955(8)	2.99(1)
O(3)	*79.7(3)*	*112.7(3)*	2.157(8)	3.07(1)	4.30(1)	2.92(1)
O(5)	*83.9(2)*	*85.4(3)*	*90.4(3)*	2.170(7)	3.00(1)	4.28(1)
O(5)[iv]	*82.3(3)*	*84.9(3)*	*161.9(3)*	*86.8(3)*	2.197(8)	3.30(1)
O(6)	*104.0(3)*	*87.9(3)*	*85.8(3)*	*170.4(2)*	*99.5(3)*	2.128(7)

Mn(2)–Mn(2)	3.174(4)	Mn(2)–O(5)–Mn(2)	93.2(3)
Mn(1)–Mn(2)	2x 3.373(3)	Mn(1)–O(1)–Mn(2)	98.5(3)
		Mn(1)–O(3)–Mn(2)	101.1(3)

$P(1)O_4$ tetrahedron

P(1)	O(1)[iv]	O(1)[v]	O(2)	O(2)[iii]
O(1)[v]	1.533(8)	2.50(1)	2.55(1)	2.512(9)
O(1)[vi]	*109.6(6)*	1.533(8)	2.512(9)	2.55(1)
O(2)	*111.2(3)*	*108.6(4)*	1.560(8)	2.52(2)
O(2)[iii]	*108.6(4)*	*111.2(3)*	*107.6(6)*	1.560(8)

$P(2)O_4$ tetrahedron

P(2)	O(3)[vi]	O(4)[vii]	O(5)	O(6)[vii]
O(3)[vii]	1.528(7)	2.561(8)	2.494(9)	2.51(1)
O(4)[vii]	*109.8(5)*	1.601(8)	2.55(1)	2.53(1)
O(5)	*110.1(4)*	*109.9(4)*	1.516(8)	2.49(1)
O(6)[vii]	*110.0(4)*	*107.5(4)*	*109.5(5)*	1.538(8)

Ag atom environments

Ag(1)–O(6)	2x 2.397(6)	O(6)–Ag(1)–O(6)	84.7(2)
Ag(1)–O(6)	2x 2.539(8)	O(6)–Ag(1)–O(6)	90.6(2)
Ag(1)–O(1)	2x 2.88(1)		
Ag(1)–O(5)	2x 3.04(1)		
Ag(2)–O(6)	2x 2.340(5)	O(6)–Ag(2)–O(6)	86.8(2)
Ag(2)–O(6)	2x 2.498(8)	O(6)–Ag(2)–O(6)	92.9(2)
Ag(2)–O(3)	2x 2.85(1)		
Ag(2)–O(1)	2x 3.22(2)		

Ag(1)–Ag(2)	0.37(2)	Ag(1)–Ag(1)	3.475(7)
Ag(1)–Ag(2)	3.385(4)	Ag(2)–Ag(2)	3.335(2)

Note. Symmetry code: (i) $x - 0.5, y - 0.5, z$; (ii) $-x + 0.5, y - 0.5, -z + 0.5$; (iii) $-x, y, -z + 0.5$; (iv) $-x + 0.5, -y + 1.5, -z + 1$; (v) $x - 0.5, -y + 1.5, z - 0.5$; (vi) $-x + 0.5, -y + 1.5, -z$; (vii) $-x + 0.5, y + 0.5, -z + 0.5$.

is the rhombic $A(2)$ site that accepts additional cations in the alluaudite structure, after the $A(1)$ site is fully occupied. Curiously, however, this has been confirmed only in the recently reported Cu-containing alluaudite (6), where two-coordinate Cu^+ resides in this site. In contrast, in $Na_2Fe_3(PO_4)_3$ (5) and in the protonated alluaudites, this $A(2)$ site has become so irregular, with two extremely short distances of ~1.8 Å (Table 7), that the square planar $A(2)'$ site, with four oxygen atoms at more regular distances, is preferred. The case of $AgMn_3(PO_4)(HPO_4)_2$ is further complicated by the splitting of the $A(2)'$ site into two closely separated ones, Ag(1) and Ag(2). Because they are only 0.37(2) Å apart, these sites probably represent local potential minima between which

TABLE 6
Alkali or Pseudo-Alkali Sites in Some Alluaudites $X(2)X(1)M(1)M(2)_2(PO_4)_3$

Compound	Tunnel 2 (0, 0, z)	Tunnel 1 ($\frac{1}{2}$, 0, z)
$[]Na^+Mn^{2+}(Fe^{3+})_2(PO_4)_3$	[] in 0, 0, 0	Na^+ in $\frac{1}{2}$, 0, 0
$[]Na^+Cd^{2+}(In^{3+})_2(PO_4)_3$	[] in 0, 0, 0	Na^+ in $\frac{1}{2}$, 0, 0
$Na^+Na^+Fe^{2+}(Fe^{3+}_{0.5}Fe^{2+}_{0.5})_2(PO_4)_3$	Na^+ in 0, ε,$^{3/4a}$	Na^+ in $\frac{1}{2}$, 0, 0
$Na^+(H^+)_2Mn^{2+}(Mn^{2+})_2(PO_4)_3$	Na^+ in 0, ε,$^{3/4a}$	O–H ··· O bridges
$Ag^+(H^+)_2Mn^{2+}(Mn^{2+})_2(PO_4)_3$	Ag^+ in 0, ε,$^{3/4}$ (two sites)^a	O–H ··· O bridges
$Na^+(H^+)_2(Fe^{2+})_2(PO_4)_3$	Na^+ in 0, ε,$^{3/4a}$	O–H ··· O bridges
$(Cu^+, Cu^{2+})_{1.35}(Fe^{2+}, Fe^{3+})_3(PO_4)_3$	Cu^+ in 0, 0, 0^b	Cu^{2+} in $\frac{1}{2}$, ε, $\frac{3}{4}$ and near $\frac{1}{2}$, 0, 0^b

[a] ε is a small positive number.
[b] An origin shift (0, $\frac{1}{2}$, 0) must be applied to the originally reported coordinates (Ref. (6)).

the polarizable Ag cations can easily migrate. According to the crystal structure determination, the Ag cations are distributed almost equally between the two sites at an occupancy of roughly 50%, with perhaps a slight preference for the more off-centered Ag(1) site (Table 4). These two sites lead to Ag–O distances ranging from 2.397(6) to 2.539(8) Å for Ag(1) and from 2.340(5) to 2.498(8) Å for Ag(2). Other relevant distances and angles of Ag(1) and Ag(2) environments are given in Table 5.

During our survey of the known alluaudites, we came across the compound previously formulated as $NaFe_3(PO_4)_3$ (4). Since our analysis has already shown that there are discernable differences between the protonated and nonprotonated series of alluaudites (Tables 6 and 7),

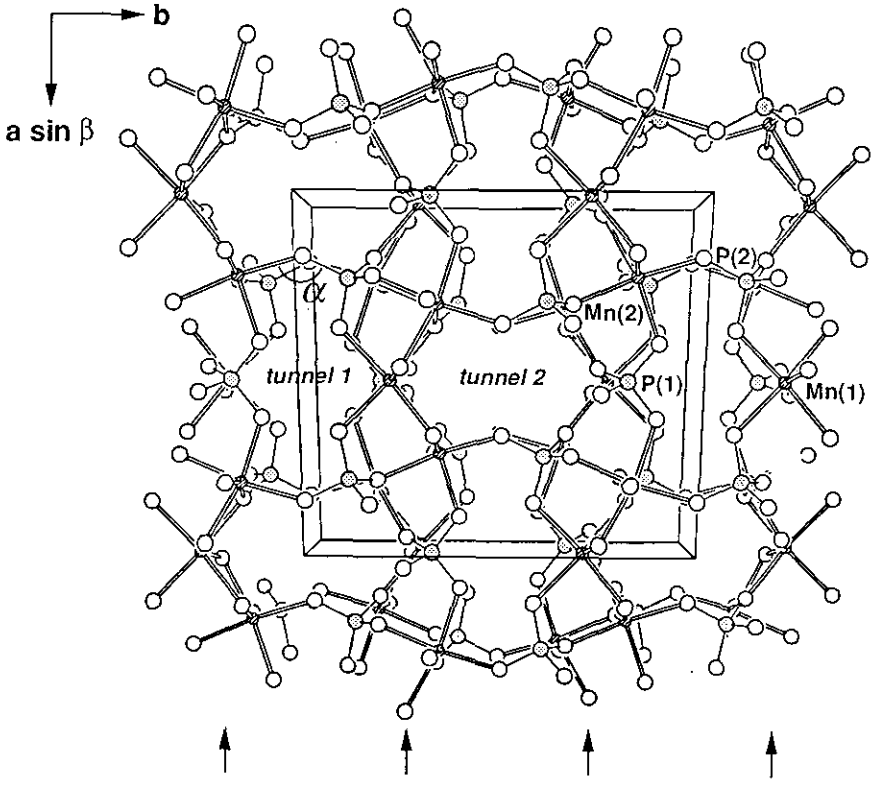

FIG. 1. View of the covalent framework of $AgMn_3(PO_4)(HPO_4)$ along c, showing the cell outline. The small hatched circles are Mn atoms, the stippled circles are P atoms, and the open circles are O atoms. The arrows indicate the alignment of sheets lying parallel to the (010) plane. The framework defines tunnels 1 and 2 in which additional cations reside. The angle α is ⟨(Mn(2)–O(6)–P(2))⟩ and is a measure of the distortion of the tunnels.

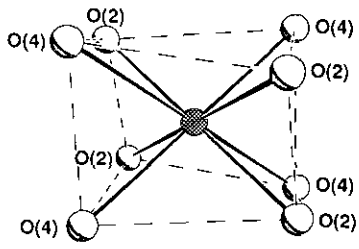

(a) cubic A(1) site (1/2, 0, 0)

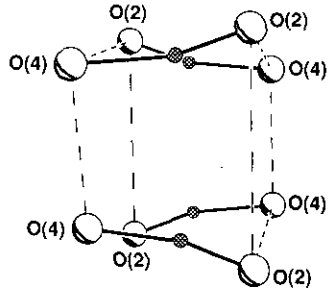

(b) O-H···O bridges

FIG. 2. Tunnel 1 contains oxygen atoms in an arrangement that may lead to (a) a cubic site at $A(1)$, or (b) occurrence of hydrogen bonds.

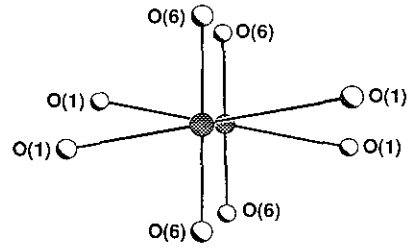

(a) rhombic A(2) site (0, 0, 0)

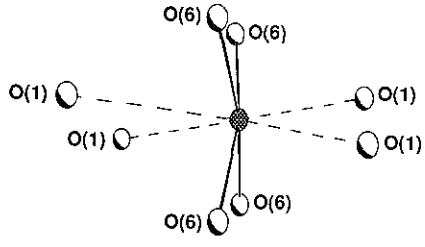

(b) square planar A(2)' site (0, ε, 3/4)

FIG. 3. Tunnel 2 contains oxygen atoms in an arrangement that may lead to (a) a rhombic site at $A(2)$, or (b) a square planar site at $A(2)'$.

we suspected that this compound was really $NaH_2Fe_3(PO_4)_3$. Examination of relevant bond distances immediately revealed some anomalies. First, one of the P–O bonds in the $P(2)O_4$ tetrahedron is significantly longer (1.588 Å) than the other three (1.520–1.531 Å). Second, as seen in Table 7, the O(2)–O(4) distance is quite short (2.532 Å), suggesting the occurrence of an O–H ··· O bridge. In any case, a bond valence calculation shows that the Fe atoms must be in oxidation state +II, and charge balance requires the existence of additional cations, viz. H^+.

It is now apparent that the critical feature that confers flexibility to the alluaudite framework so that it can distort to accomodate the H^+ cations is given by the buckling of the Mn(2)–O(6)–P(2) angle (indicated as α in Fig. 1), at the portion of the framework where there is corner sharing (between the $Mn(2)O_6$ octahedron and the $P(2)O_4$ tetrahedron), the rest of the framework being more rigid. In the protonated alluaudites, the constriction of tunnel 1 engendered by the straddling of the O–H ··· O bridge gives rise to a Mn(2)–O(6)–P(2) angle significantly more acute (~135°) than that in the nonprotonated forms (~145°) (Table 7).

Because their ionic radii are similar (Na^+ 1.02 Å, Ag^+ 1.15 Å) (17), it is possible to substitute the Na cation in the $NaMn_3(PO_4)(HPO_4)_2$ structure by Ag. The Ag cation, being relatively polarizing, is able to support the off-centered square planar coordination in sites $A(2)'$. That sub-

TABLE 7
Comparison of Selected Distances (Å) and Angles (°) in Some Alluaudites[a]

Compound	$A(2)$–O(6)[b]	$A(2)$–O(1)[b]	O(2)–O(4)	α[c]	Reference
$NaMnFe_2(PO_4)_3$	2.080	2.782	3.039	145.8	1
$NaCdIn_2(PO_4)_3$	2.21	2.91	3.139	144.9	3
$Na_2Fe_3(PO_4)_3$	1.870	2.794	3.00	137.5	5
$NaMn_3(PO_4)(HPO_4)_2$	1.689	3.154	2.503	133.8	7
$AgMn_3(PO_4)(HPO_4)_2$	1.754	3.163	2.489	135.9	This work
$NaFe_3(PO_4)(HPO_4)_2$	1.693	3.113	2.532	134.7	4
$Cu_{1.35}Fe_3(PO_4)_3$	1.963	2.911	2.956	143.3	6

[a] Standard deviations are not greater than ~0.01 Å for the distances and ~0.5° for the angles.
[b] $A(2)$ is the theoretical rhombic site at 0, 0, 0 located in tunnel 2 (See Fig. 3a).
[c] The angle α, indicated in Fig. 1, is ⟨(Mn(2)–O(6)–P(2))⟩.

stitution by K or Tl (K^+ 1.38 Å, Tl^+ 1.50 Å) has thus far not been achieved perhaps suggests that there is a limit to which the alluaudite framework can distort. The Mn(2)–O(6)–P(2) angle is fixed by the O–H $\cdots$ O distance in tunnel 1, fixing the size of tunnel 2, and thus larger cations must enter the $A(2)'$ site in tunnel 2 at increasingly off-center positions (i.e., larger ε in 0, ε, $\frac{3}{4}$).

With the recognition of the true formula of the all-Fe compound, there are now three examples of completely unoxidized, protonated members of the alluaudite series: $NaH_2Mn^{2+}(Mn^{2+})_2(PO_4)_3$, $AgH_2Mn^{2+}(Mn^{2+})_2(PO_4)_3$, and $NaH_2Fe^{2+}(Fe^{2+})_2(PO_4)_3$. Thermal gravimetric analysis shows that $AgMn_3(PO_4)(HPO_4)_2$ undergoes a thermal degradation corresponding to a dehydroxylation process with the loss of one water molecule per formula unit. This degradation takes place at a temperature higher (480°C) than that (450°C) in $NaMn_3(PO_4)(HPO_4)_2$ (7). Further experiments are in progress to perform different substitutions in the alluaudite series. Moreover, it would be interesting to see if $AgMn_3(PO_4)(HPO_4)_2$ is susceptible to ionic conduction.

ACKNOWLEDGMENT

A.M. thanks NSERC Canada for financial support in the form of a postdoctoral fellowship.

REFERENCES

1. P. B. Moore, *Am. Mineral.* **56,** 1955 (1971).
2. P. B. Moore and J. Ito, *Mineral. Mag.* **43,** 227 (1979).
3. D. Antenucci, G. Miehe, P. Tarte, W. W. Schmahl, and A.-M. Fransolet, *Eur. J. Mineral.* **5,** 207 (1993).
4. D. R. Corbin, J. F. Whitney, W. C. Fultz, G. D. Stucky, M. M. Eddy, and A. K. Cheetham, *Inorg. Chem.* **25,** 2279 (1986).
5. O. V. Yakubovich, M. A. Simonov, Y. K. Egorov-Tismenko, and N. V. Belov, *Dokl. Akad. Nauk SSSR* **236,** 1123 (1977).
6. T. E. Warner, W. Milius, and J. Maier, *J. Solid State Chem.* **106,** 301 (1993).
7. F. Leroux, A. Mar, C. Payen, D. Guyomard, A. Verbaere, and Y. Piffard, *J. Solid State Chem,* in press.
8. M. Tsuji, S. Komarneni, Y. Tamaura, and M. Abe, *Mater. Res. Bull.* **27,** 741 (1992).
9. Y. Cudennec, A. Riou, and Y. Gérault, *C.R. Acad. Sci. Paris Ser. 2* **302,** 1149 (1986).
10. P. B. Moore and T. Araki, *Am. Mineral.* **58,** 302 (1973).
11. S. Menchetti and C. Sabelli, *Acta Crystallogr. Sect. B* **29,** 2541 (1973).
12. Y. Gérault, A. Riou, and Y. Cudennec, *Acta Crystallogr. Sect. C* **43,** 1829 (1987).
13. K. Yvon, W. Jeitschko, and E. Parthé, *J. Appl. Crystallogr.* **10,** 73 (1977).
14. G. M. Sheldrick, "SHELXTL PLUS 4.0," Siemens Analytical X-Ray Instruments, Inc., Madison, WI, 1990.
15. N. E. Brese and M. O'Keeffe, *Acta Crystallogr. Sect. B* **47,** 192 (1991).
16. I. D. Brown and D. Altermatt, *Acta. Crystallogr. Sect. B* **41,** 244 (1985).
17. R. D. Shannon, *Acta Crystallogr. Sect. A.* **32,** 751 (1976).